ACADEMIC PRESS

Available online at www.sciencedirect.com

SCIENCE DIRECT®

Journal of Sound and Vibration 265 (2003) 953–966

JOURNAL OF SOUND AND VIBRATION

www.elsevier.com/locate/jsvi

Interpreting proper orthogonal modes of randomly excited vibration systems

B.F. Feeny*, Y. Liang

Department of Mechanical Engineering, Michigan State University, 2555 Engineering Building, East Lansing, MI 48824, USA

Received 7 May 2001; accepted 18 August 2002

Abstract

Proper orthogonal modes (POMs) of displacements are interpreted for linear vibration systems under random excitation. Excitations are considered for which the Fourier transform is convergent, meaning that the input must have zero mean, and no sustained sinusoidal component. In such a case, the POMs in undamped discrete linear symmetric systems can represent linear natural modes if the mass distribution is known. POMs in one-dimensional distributed-parameter self-adjoint systems can approximately represent the linear normal modes if the mass distribution is known. Simulation examples are presented. Simulations show that these ideas are also applicable under light modal damping.
© 2002 Elsevier Science Ltd. All rights reserved.

1. Introduction

This paper regards the application of proper orthogonal decomposition (POD) for experimental modal analysis of homogeneous systems under random excitations.

POD, primarily a statistical formulation, has emerged as a useful experimental tool in dynamics and vibration. The discrete formulation resembles singular-value decomposition. Our interest is in the application of POD to the sensed displacements, $x_1(t), x_2(t), \ldots, x_M(t)$, at M locations on a structure. When the displacements are sampled N times at a fixed sampling rate, we can form displacement-history arrays, such that $\mathbf{x}_i = (x_i(t_1), x_i(t_2), \ldots, x_i(t_N))^{\mathrm{T}}$, for $i = 1, \ldots, M$. The mean values are often subtracted from the displacement histories. In performing the POD, these displacement histories are used to form an $N \times M$ ensemble matrix,

$$\mathbf{X} = [\mathbf{x}_1, \mathbf{x}_2, \ldots, \mathbf{x}_M].$$

*Corresponding author. Tel.: +1-517-353-9451; fax: +1-517-353-1750.
E-mail address: feeny@me.msu.edu (B.F. Feeny).

0022-460X/03/$ - see front matter © 2002 Elsevier Science Ltd. All rights reserved.
doi:10.1016/S0022-460X(02)01265-8

Each row of $\mathbf{X}$ represents a point in the co-ordinate space at a particular instant in time. The $M \times M$ correlation matrix $\mathbf{R} = (1/N)\mathbf{X}^{\mathrm{T}}\mathbf{X}$ is then formed. (If means are removed from the signals, then $\mathbf{R}$ is the covariance matrix, although the divisor should be the statistical degree of freedom $N-1$ rather than N.) Since $\mathbf{R}$ is real and symmetric, its eigenvectors form an orthogonal basis. The eigenvectors of $\mathbf{R}$ are the proper orthogonal modes (POMs), and the eigenvalues are the proper orthogonal values (POVs). In the analysis of turbulence, the POMs have been shown to represent the optimal distributions of kinetic energy or power, and the POVs indicate the power associated with these principal distributions [1,2]. Alternatively, the POMs represent the principal axes of inertia of the data in the measurement space, while the POVs values indicate the mean-squared values of the data in each axis [3].

The method was applied to turbulence by Lumley [4,5], and has since received considerable attention from structural dynamicists. POD has been useful in uncovering spatial coherence in turbulence [4,5,1] and structures [2,6], determining the number of active state variables in a system [1,2,6], and in uncovering modal interactions [7,8]. Proper orthogonal modes have been treated as empirical modal bases for discretizing non-linear partial differential equations by Galerkin projections in turbulence applications [1] and in structural dynamics [9–14], and also for system identification [15,16].

Cusumano and Bai [6], Davies and Moon [7] and Kust [17] observed that the POMs in their non-linear structures resembled the normal modes of the linearized system. A recent analysis has shown that the POMs may indeed converge to linear normal modes (LNMs) in multi-modal free responses of symmetric linear systems, but *only* if the mass matrix has the form $m\mathbf{I}$ (which can be achieved by a co-ordinate transformation if the mass distribution is known) and if the system is lightly damped [3]. This conclusion was also reached with the perspective of singular-value decomposition [18] and time correlation [25]. Furthermore, the POMs of discretized continuous one-dimensional systems with lightly damped multi-modal free responses converge *in approximation* to the discretized LNMs, again if the mass distribution can be cast as uniform, and if the discretization is spatially uniform [19]. This result has been tested experimentally [20,21], and extended to non-uniform discretizations through a weighted POD [21]. These results provide a fundamental tie between the statistically derived POMs and the geometrically based LNMs in certain discrete systems.

If POD is to be realized as a viable approach for experimental modal analysis, certain issues must be overcome. Among the current limitations are the known mass-distribution requirement, and the restriction to multi-modal free responses. In this paper, we address the latter restriction. We extend the applicability of POD as a modal analysis tool to uniform-mass systems undergoing random excitation.

Kerschen and Golinval [18] had addressed POD in randomly excited systems cast in state variable form with a controller. They found that the state-variable correlation matrix represented the controllability Grammian. In this paper, we look at the POMs from the displacement ensemble of vibration systems, and tie POMs to LNMs under certain circumstances.

In what follows, we summarize the analysis of POD in vibration systems, both discrete and continuous. We then incorporate responses to a class of random excitations and show that the POMs converge to the linear natural modes. We finally provide simulation examples.

2. POD of multi-modal vibrations

First, we summarize the basic results needed to make our interpretations. The previous analysis approach of POD applied to impulse responses for discrete parameter systems [3] and for continuous parameter systems [19] can be used for the random responses. The seed of the result lies in the normal mode shapes, and what we change here is the response of the modal co-ordinates. In the previous works, the modal co-ordinates were treated with a free response. Here, they are treated as a random response.

Next, we summarize the role played by the mode shapes for both lumped-parameter and distributed-parameter systems. We then address the role of the modal-co-ordinate response under random excitation.

2.1. Lumped-parameter linear systems

The equations of motion of an undamped, unforced, symmetric M-degree-of-freedom system of the form $\mathbf{M}\ddot{\mathbf{y}} + \mathbf{K}\mathbf{y} = \mathbf{0}$ can be rewritten through the co-ordinate transformation $\mathbf{y} = \mathbf{M}^{-1/2}\mathbf{x}$ as

$$\ddot{\mathbf{x}} + \mathbf{A}\mathbf{x} = \mathbf{0}, \tag{1}$$

where $\mathbf{A} = \mathbf{M}^{-1/2}\mathbf{K}\mathbf{M}^{-1/2}$ is symmetric [22]. The response can be written in terms of the modes, such that

$$\mathbf{x}(t) = \mathbf{V}\mathbf{q}(t), \tag{2}$$

where $\mathbf{V} = [\mathbf{v}_1, \ldots, \mathbf{v}_M]$ is the modal matrix of M normal modes, and $\mathbf{q}(t)$ is the vector of modal co-ordinates $q_i(t)$.

Then the ensemble matrix has the form

$$\mathbf{X} = [\mathbf{x}(t_1)\cdots\mathbf{x}(t_N)]^{\mathrm{T}} = (\mathbf{V}\mathbf{Q}^{\mathrm{T}})^{\mathrm{T}} = \mathbf{Q}\mathbf{V}^{\mathrm{T}},$$

where $\mathbf{Q}^{\mathrm{T}} = [\mathbf{q}(t_1), \mathbf{q}(t_2), \ldots, \mathbf{q}(t_N)]$; as such, $\mathbf{Q}$ is the modal ensemble matrix. The correlation matrix then has the form

$$\mathbf{R} = \frac{1}{N}\mathbf{X}^{\mathrm{T}}\mathbf{X} = \frac{1}{N}\mathbf{V}\mathbf{Q}^{\mathrm{T}}\mathbf{Q}\mathbf{V}^{\mathrm{T}}.$$

We can check whether a modal vector is actually a POM by post-multiplying the matrix $\mathbf{R}$ by a modal vector. Thus,

$$\mathbf{R}\mathbf{v}_j = \frac{1}{N}\mathbf{V}\mathbf{Q}^{\mathrm{T}}\mathbf{Q}\mathbf{V}^{\mathrm{T}}\mathbf{v}_j.$$

The vector $\mathbf{V}^{\mathrm{T}}\mathbf{v}_j$ has elements $\mathbf{v}_i^{\mathrm{T}}\mathbf{v}_j$. Since the mass matrix is $\mathbf{I}$ in Eq. (1), the orthogonality relation $\mathbf{v}_i^{\mathrm{T}}\mathbf{v}_j = \delta_{ij}$ reduces the matrix product to

$$\mathbf{R}\mathbf{v}_j = \frac{1}{N}\mathbf{V}\mathbf{Q}\mathbf{Q}^{\mathrm{T}}\mathbf{h}_j,$$

where $\mathbf{h}_j = [0\cdots1\cdots0]^{\mathrm{T}}$ is a vector of zeros except for the jth element, which is one.

The matrix $\mathbf{R_Q} = (1/N)\mathbf{Q}^{\mathrm{T}}\mathbf{Q}$ has elements

$$\frac{1}{N}\sum_{k=1}^{N} q_i(t_k)q_j(t_k).$$

In the case of undamped free vibration, as long as the frequencies of the modes are distinct, each element of $\mathbf{R_Q}$ disappears as $N \to \infty$ except for the diagonal elements, which are the mean-squared values of the modal co-ordinates, $\bar{q_i^2} = E[q_i^2]$. So for free vibration, $\mathbf{R_Q} \to \mathbf{D}$, a diagonal matrix, as N gets large. Hence, $\mathbf{R}\mathbf{v}_j = \mathbf{V}\mathbf{D}\mathbf{h}_j = \bar{q_j^2}\mathbf{v}_j$. The eigenvectors of $\mathbf{R}$, and thus the POMs, converge to the modal vectors.

We are poised to examine the behavior of the $q_j(t)$ under random excitation, for which the remaining issue is whether $\mathbf{R_Q}$ diagonalizes. Before we address this, we review the application to continuous systems.

2.2. Distributed-parameter linear systems

We summarize a previous analysis of the POMs for LNMs in distributed-parameter systems [19].

The model of a one-dimensional distributed-parameter system, such as a beam or string of length l, is

$$m(x)\ddot{y} + L_1 y = 0, \tag{3}$$

where $y(x,t)$ is a displacement, the "dots" represent partial differentiation with respect to time, $m(x)$ is a known mass distribution, and L_1 is a self-adjoint linear operator. Letting $u = m^{1/2}(x)y$, the system can be rewritten as $\ddot{u} + m^{-1/2}(x)L_1 m^{-1/2}(x)u = 0$, or

$$\ddot{u} + L_2 u = 0. \tag{4}$$

L_2 is self-adjoint. For this system with its boundary conditions, separation of variables leads to eigenvalues and eigenfunctions $\phi_i(x)$ which can be normalized such that

$$\int_0^L \phi_i(x)\phi_j(x)\,\mathrm{d}x = \delta_{ij}. \tag{5}$$

The absence of the mass in this integral is critical for connecting the POMs to LNMs.

Suppose we have a set of displacement measurements $u(x,t)$ of the system, sampled at co-ordinates $x_1, \ldots, x_M$. This leads to a set of measurements $\mathbf{u} = [u(x_1,t)\cdots u(x_M,t)]^{\mathrm{T}}$. Then $u(x,t) \approx \sum_{i=1}^{\hat{M}} q_i(t)\phi_i(x) = \boldsymbol{\phi}^{\mathrm{T}}\mathbf{q}$, where $\boldsymbol{\phi} = [\phi_1(x)\cdots\phi_{\hat{M}}(x)]^{\mathrm{T}}$ is a vector of the modal functions, and $\mathbf{q}(t) = [q_1(t)\cdots q_{\hat{M}}(t)]^{\mathrm{T}}$ is the vector of modal co-ordinates. We will take $\hat{M} = M$ in this discussion. We define a matrix $\boldsymbol{\Phi} = [\mathbf{v}_1\cdots\mathbf{v}_M] = [\boldsymbol{\phi}(x_1)\cdots\boldsymbol{\phi}(x_M)]^{\mathrm{T}}$. Thus, the vectors $\mathbf{v}_i = [\phi_i(x_1)\cdots\phi_i(x_M)]^{\mathrm{T}}$ are spatial discretizations of the mode shapes $\phi_i(x)$. Then

$$\mathbf{u} = \boldsymbol{\Phi}\mathbf{q}(t)$$

relates the discrete displacements of the beam to the discretizations of the mode shapes.

The displacements are sampled at time $t_1, \ldots, t_N$. We construct an $N \times M$ ensemble matrix $\mathbf{U} = [\mathbf{u}(t_1)\cdots\mathbf{u}(t_N)]^{\mathrm{T}} = [\boldsymbol{\Phi}\mathbf{q}(t_1)\cdots\boldsymbol{\Phi}\mathbf{q}(t_N)]^{\mathrm{T}}$, or

$$\mathbf{U} = (\boldsymbol{\Phi}\mathbf{Q}^{\mathrm{T}})^{\mathrm{T}} = \mathbf{Q}\boldsymbol{\Phi}^{\mathrm{T}},$$

where again $\mathbf{Q}^{\mathrm{T}} = [\mathbf{q}(t_1)\cdots\mathbf{q}(t_N)]$ is an $M \times N$ matrix. The correlation matrix can thus be built as $\mathbf{R} = (1/N)\mathbf{U}^{\mathrm{T}}\mathbf{U} = (1/N)\boldsymbol{\Phi}\mathbf{Q}^{\mathrm{T}}\mathbf{Q}\boldsymbol{\Phi}^{\mathrm{T}}$.

We now check whether $\mathbf{v}_j$ is an eigenvector of $\mathbf{R}$ by examining $\mathbf{R}\mathbf{v}_j = (1/N)\boldsymbol{\Phi}\mathbf{Q}^{\mathrm{T}}\mathbf{Q}\boldsymbol{\Phi}^{\mathrm{T}}\mathbf{v}_j$. The quantity $\boldsymbol{\Phi}^{\mathrm{T}}\mathbf{v}_j$ has elements $\mathbf{v}_i^{\mathrm{T}}\mathbf{v}_j$. We assume now that the spatial discretization is evenly spaced. (A weighted POD has been formulated for unevenly spaced discretizations [21].) Then, $\mathbf{v}_i^{\mathrm{T}}\mathbf{v}_j = \sum_{k=1}^{M}\phi_i(x_k)\phi_j(x_k) \approx (1/h)\int_0^L \phi_i(x)\phi_j(x)\,\mathrm{d}x$ by the rectangular rule, where h is the spacing of the spatial discretization. Thus we approximate $\mathbf{v}_i^{\mathrm{T}}\mathbf{v}_j \approx (1/h)\delta_{ij}$. If this approximation is reasonable, then the quantity $\boldsymbol{\Phi}^{\mathrm{T}}\mathbf{v}_j \approx [0\cdots 0, 1/h, 0\cdots 0]^{\mathrm{T}} = \mathbf{h}_j$ has elements of approximately zero, except the jth element which is approximately $1/h$. The error associated with the rectangular integration representation of the underlying orthogonality integral is on the order of kh^3, where k is proportional to a characteristic curvature in the integrand [23]. Then $\mathbf{R}\mathbf{v}_j \approx (1/N)\boldsymbol{\Phi}\mathbf{Q}^{\mathrm{T}}\mathbf{Q}\mathbf{h}_j$. The ijth elements of $\mathbf{R}_{\mathbf{Q}} = (1/N)\mathbf{Q}^{\mathrm{T}}\mathbf{Q}$ are $(1/N)\sum_{k=1}^{N} q_i(t_k)q_j(t_k)$.

Again, in the multi-modal free vibration case [19], $q_i(t)$ and $q_j(t)$ with distinct frequencies lead to

$$\lim_{N\to\infty} \frac{1}{N}\mathbf{Q}^{\mathrm{T}}\mathbf{Q} = \mathbf{D},$$

which is diagonal with elements $d_{ii} = \sum_{k=1}^{N} q_i(t_k)^2/N$, which are the mean-squared values of $q_i(t)$.

In such case, $\mathbf{R}\phi_j$ converges approximately to $\boldsymbol{\Phi}\mathbf{D}\mathbf{h}_j = \boldsymbol{\Phi}\mathbf{h}_j d_{jj} = \mathbf{v}_j d_{jj}/h$. So, for large N, with evenly spaced data and distinct modal frequencies, the POMs converge approximately to $\mathbf{v}_j$, which are the discretized linear modes. In other words the POMs converge to $\mathbf{v}_j + \mathbf{e}_j$ where $\mathbf{e}_j$ is an error vector. Furthermore, the POVs converge to d_{jj}/h, which is proportional to the mean-squared modal co-ordinate.

In this work, we examine the effect of modal co-ordinates under random excitation. Again, the remaining issue is whether $\mathbf{R}_{\mathbf{Q}}$ diagonalizes.

2.3. Modal responses under random excitation

Here, we extend the connection between the POMs and the LNMs to the case of zero-mean random excitation. The goal here is to verify that the modal ensemble matrix $\mathbf{R}_{\mathbf{Q}} = (1/N)\mathbf{Q}^{\mathrm{T}}\mathbf{Q}$ is nearly diagonal, in both lumped mass and continuous parameter systems. If this is the case, then the same conclusions can be drawn as for the multi-modal free response cases.

In the lumped parameter models, the modal equations of motion are

$$\ddot{\mathbf{x}} + \mathbf{A}\mathbf{x} = \mathbf{F}(t), \tag{6}$$

and the continuous parameter model is

$$\ddot{u} + L_2 u = F(x,t). \tag{7}$$

Modal analysis can be applied in both cases to yield a set of modal equations of the form

$$\ddot{q}_i + \omega_i^2 q_i = f_i(t), \tag{8}$$

where $f_i(t) = \mathbf{v}_i^{\mathrm{T}}\mathbf{F}(t)$ for the lumped parameter case, and $f_i(t) = \int_0^l \phi_i(x)F(x,t)\,\mathrm{d}x$ for the continuous parameter case, where i is an index for the modes. Taking the Fourier transform of Eq. (8), we can write

$$\tilde{q}_i(\omega) = \tilde{H}_i(\omega)\tilde{F}_i(\omega), \tag{9}$$

provided the Fourier transform $\tilde{F}_i(\omega)$ converges. If $f_i(t)$ has a constant component or a sustained sinusoid, the Fourier transform does not converge (although it can be represented with Dirac delta functions). Thus, we exclude these excitations. As such, we consider random excitations with convergent, or bounded, Fourier transforms.

The solution to Eq. (8) is thus

$$q_i(t) = \int_{-\infty}^{t} h_i(t-\tau) f_i(\tau)\,\mathrm{d}\tau = \int_{-\infty}^{\infty} h_i(t-\tau) f_i(\tau)\,\mathrm{d}\tau, \tag{10}$$

where $h_i(t)$ is the unit impulse response of the ith modal co-ordinate, and can be represented as the inverse Fourier transform of $\tilde{H}_i(\omega)$. The form of Eq. (10) takes advantage of the fact that $h_i(t) = 0$ for $t<0$ [24]. Time series are finite in practice. If the excitation starts at $t = 0$, then we can write

$$q_i(t) = \int_{0}^{\infty} h_i(t-\tau) f_i(\tau)\,\mathrm{d}\tau. \tag{11}$$

In application to the POD problem in the preceding sections, our concern is whether the correlation matrix $\mathbf{R_Q} = (1/N)\mathbf{Q}^{\mathrm{T}}\mathbf{Q}$ converges to a diagonal matrix with increasing N. The elements of $\mathbf{R_Q}$ are

$$r_{ij} = \frac{1}{N}\sum_{k=1}^{N} q_i(t_k) q_j(t_k) = \frac{1}{N}\sum_{k=1}^{N} \int_0^{\infty} f_i(\tau) h_i(t_k-\tau)\,\mathrm{d}\tau \int_0^{\infty} f_j(\theta) h_j(t_k-\theta)\,\mathrm{d}\theta. \tag{12}$$

Exchanging the order of the sums, we have

$$r_{ij} = \int_0^{\infty}\int_0^{\infty} f_i(\tau) f_j(\theta) \left[\frac{1}{N}\sum_{k=1}^{N} h_i(t-\tau) h_j(t-\theta)\right] \mathrm{d}\tau\,\mathrm{d}\theta. \tag{13}$$

Assuming $\zeta_i = \zeta_j = 0$, and $\omega_i \neq \omega_j$, then

$$\lim_{N\to\infty} \frac{1}{N}\sum_{k=1}^{N} h_i(t-\tau) h_j(t-\theta) = d_i(\tau,\theta)\delta_{ij}, \tag{14}$$

where $d_i(\tau,\theta)$ is defined by Eq. (14). As such, we have $r_{ij} \to r_i\delta_{ij}$. Referring to Eq. (12) for the case of $i = j$, we can see that $r_i = E[q_i^2]$ is the mean-squared value of the modal co-ordinate q_i.

Hence, for undamped systems with distinct modal frequencies and random excitations with convergent Fourier transforms, we expect the modal correlation matrix $\mathbf{R_Q}$ to diagonalize. In practice, with a finite but "large" N, we expect $\mathbf{R_Q} \approx \mathbf{D}$, where $\mathbf{D}$ is diagonal with diagonal elements equal to the mean-squared values of the modal co-ordinates. Furthermore, systems with "light" modal damping and finite N should "nearly" diagonalize, with dominant diagonal elements.

With the diagonalization of $\mathbf{R_Q}$, the POMs converge to the LNMs in the lumped parameter case, and the POMs converge to approximations of the LNMs in the continuous parameter case.

2.4. Remarks

The above analysis ties the statistically formulated POMs to the discretization of the linear normal modes for multi-modal random responses of undamped systems with known mass distributions. As long as the Fourier transform of $F(t)$ or $F(x,t)$ is convergent, we have no

restrictions on the random excitations or their distributions. In fact, the formulation here also takes care of impulse responses, which were studied previously with the perspective of the ensuing free response.

We emphasize that the above analysis is not valid if the Fourier transform of the excitation is non-convergent. Examples of such excitations are those with non-zero mean, and those with a sustained harmonic. For example, if we consider a system excited with a constant applied force, the steady state response is constant, at the static equilibrium. The static equilibrium vector, which is generally not one of the LNMs, will be the dominant POM (if the POD is applied without subtracting the means from the signals). Furthermore, the steady state response to a pure sinusoidal excitation cannot be used to discern mode shapes (unless the input signal is incorporated into the POD [18]), although at resonance the resonating mode shape can be approximated [3].

While a constant or sustained sinusoidal component of the excitation is non-convergent in its Fourier transform, in practice, the experimenter will find that such signal components do have bounded fast Fourier transforms. The discrete fast Fourier transform is related to the Fourier series, which represents constant and sinusoidal signals with finite constants. Observing a spike in the FFT in the laboratory should be a warning that the continuous-time Fourier transform might be non-convergent. Indeed, the experimenter does not need to measure the input signal while applying POD as formulated here. However, an excitation with a non-convergent Fourier transform on the response will have an adverse effect on the modal extraction, as in the examples discussed above.

Working with finite N, it is likely that the resulting time series will not have exactly zero mean, even if a zero mean is expected. It may be advisable to remove the means from the displacement histories prior to building the ensemble matrix $\mathbf{X}$.

3. Numerical examples

We apply these ideas to the random excitation of three simple systems, a three-mass system, a cantilevered beam and a hinged–hinged beam, for which theoretical modes are readily available for comparison.

3.1. Three-mass system

In this undamped example, the mass matrix was $\mathbf{M} = \mathbf{I}$, and the stiffness matrix was

$$\mathbf{K} = \begin{bmatrix} 2 & -1 & 0 \\ -1 & 2 & -1 \\ 0 & -1 & 1 \end{bmatrix}.$$

This system has eigenvectors $\mathbf{v}_1 = [0.3280, 0.5910, 0.7370]^{\mathrm{T}}$, $\mathbf{v}_2 = [0.7370, 0.3280, -0.5910]^{\mathrm{T}}$, and $\mathbf{v}_3 = [0.5910, -0.7370, 0.3280]^{\mathrm{T}}$, normalized to length one, and modal frequencies $\omega_1 = 0.4450$, $\omega_2 = 1.2470$, and $\omega_3 = 1.8019$. The system was simulated with Matlab using the function 'rand' to generate a random excitation. The random excitation value was determined in the calling routine so that it remained fixed while the internal step-size adjuster was at work. Each mode was excited

uniformly, i.e., the modal excitation was $f_i(t) = \mathbf{v}_i^{\mathrm{T}}\mathbf{F}(t) = \gamma_i a(t)$ such that $\gamma_i = \gamma$. A total of 400 samples were obtained at a time step of 0.14, resulting in four first-mode periods of data. The mean was removed from the response. The resulting POMs were $\mathbf{u}_1 = [0.3254, 0.5899, 0.7390]^{\mathrm{T}}$, $\mathbf{u}_2 = [0.7547, 0.3088, -0.5788]^{\mathrm{T}}$, and $\mathbf{u}_3 = [0.5697, -0.7461, 0.3447]^{\mathrm{T}}$, normalized to length one. The magnitudes of the errors were thus 0.0035, 0.0288, and 0.0286.

3.2. Beam examples

For each numerical simulation, we chose a uniform mass per unit length of $m(x) = 1$, a stiffness of $EI = 1$, and a length of $L = 1$. Simulations were performed on 10 normal modal co-ordinates with a random excitation defined as in the previous example, and zero damping. Each mode was excited uniformly, i.e., the modal excitation was $f_i(t) = \int_0^l \phi_i(x)F(x,t)\,\mathrm{d}x = \gamma_i a(t)$ such that $\gamma_i = \gamma$.

For the numerical simulation of the cantilevered beam, the clamp was at $x = 0$. For this case, the modal functions are $\cosh(\beta_i x) - \cos(\beta_i x) - \sigma_i(\sinh(\beta_i x - \sin(\beta_i x))$, where the successive values of β_i are 1.87510407, 4.69409113, 7.85475744, 10.99554073, 14.13716839, and $(2i-1)\pi/2$ for $i > 5$, and the values of σ_i are 0.7341, 1.0185, 0.9992, and 1.0000 for $i > 3$ [22]. The modal frequencies are $\omega_i = \beta_i^2\sqrt{EI/m}$.

The displacements were expanded in a truncated modal series consisting of the first 10 normal modes. The beam was then "sampled" at 10 equally spaced locations from $x = 0.1$ to 1. The vibrations were sampled through approximately four fundamental periods at an interval of $\Delta t = 0.018$, resulting in 400 time samples.

The success depends on the rectangular-rule inner-product approximation of Eq. (5). With the current discretization, the rectangular rule uses end values as opposed to midpoints. The discrete inner products times h of the first five discretized modal vectors are given in Table 1, from which the approximation of orthogonality can be judged.

Fig. 1 shows the comparison between the first four discretized linear normal modes along with the POMs computed under the circumstances given. The norms of the errors between these first five sets of normalized modes and the corresponding POMs were 0.0001, 0.1820, 0.2636, 0.0835, and 0.0713.

The quality of the results may vary with the situation. Trouble is expected when the amplitudes of two or more modes are very similar [3], since the eigenvectors of repeated eigenvalues $\mathbf{R}$ are then non-uniquely oriented.

We have also applied the method to a hinged–hinged beam. In putting 10 "sensors" on the beam away from the endpoints, at the midpoints of 10 equal intervals, the spacing was $h = 1/11$.

Table 1
Inner products times h between the first five discretized natural modes of the cantilever beam

	$\mathbf{v}_1$	$\mathbf{v}_2$	$\mathbf{v}_3$	$\mathbf{v}_4$	$\mathbf{v}_5$
$\mathbf{v}_1$	1.0000	−0.1812	0.1949	0.0342	−0.0007
$\mathbf{v}_2$	−0.1812	1.0000	−0.2001	0.0186	−0.0338
$\mathbf{v}_3$	0.1949	−0.2001	1.0000	−0.0559	0.0619
$\mathbf{v}_4$	0.0342	0.0186	−0.0559	1.0000	−0.0319
$\mathbf{v}_5$	−0.0007	−0.0338	0.0619	−0.0319	1.0000

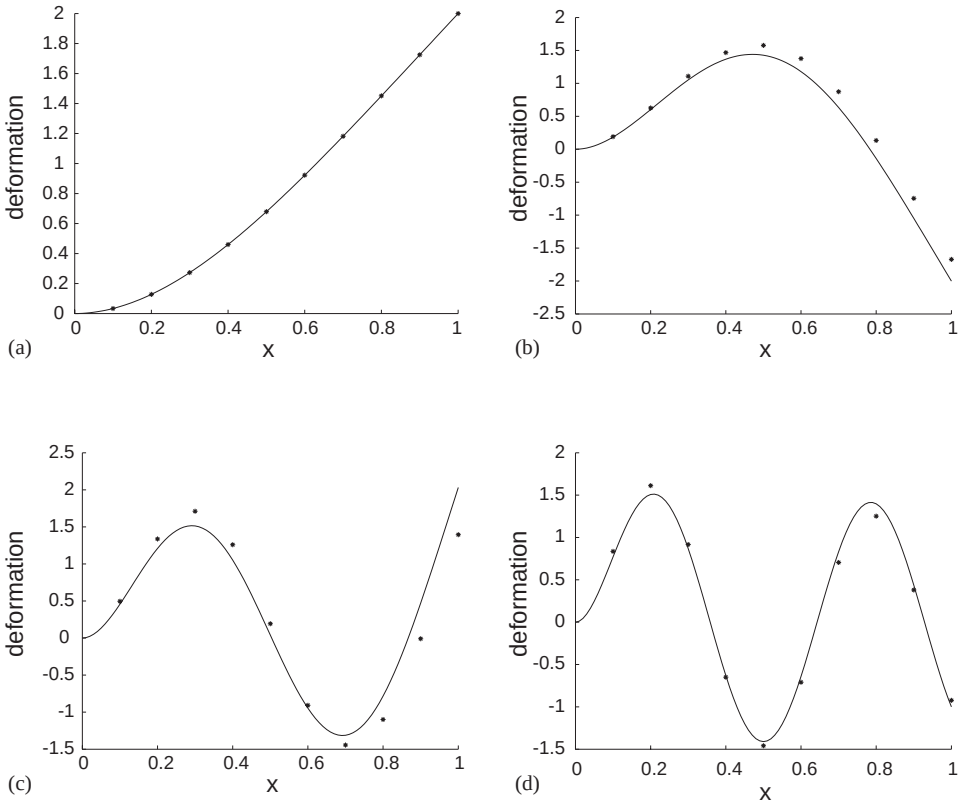

Fig. 1. The first four LNMs of an undamped cantilevered beam are plotted with solid lines, '—'. The corresponding POMs are plotted with symbols, '∗'. (a) First mode, (b) second mode, (c) third mode, and (d) fourth mode.

Here, the modal functions are $\phi_i(x) = \sin(i\pi x)$. The inner products between the discretized modal vectors are, to at least four decimal points, $\mathbf{v}_i^{\mathrm{T}}\mathbf{v}_j = \delta_{ij}/h$. The modal frequencies, $\omega_i = i\pi$, are distinct and well spaced.

The vibrations were sampled through 400 time samples at an interval of $\Delta t = 0.0063$, resulting in four fundamental periods. Again, the modal excitation was uniform. Fig. 2 shows the comparison between the first four sets of modes. The higher modes visually compared as well as those shown. The norms of the errors between these first four sets of modes were 0.0002, 0.0025, 0.0065, 0.0105, and 0.0865. The mean norm of the error between the 10 computed modes was 0.0281.

The quality of the results for both the cantilevered and hinged beams is similar as with the POD performed on impulse responses [19]. The results for the hinged beam are more accurate than the cantilevered beam. Presumably, the finite spatial resolution is responsible for deviation in the cantilevered beam. The hinged beam has sinusoidal modal functions, and as long as the spatial resolution meets the Nyquist criterion, we might expect full representation of the sinusoids.

To test the effect of spatial resolution on the cantilevered beam, we did simulations with 40 sensors. The results are improved. For a brief illustration, modes two and three are shown in

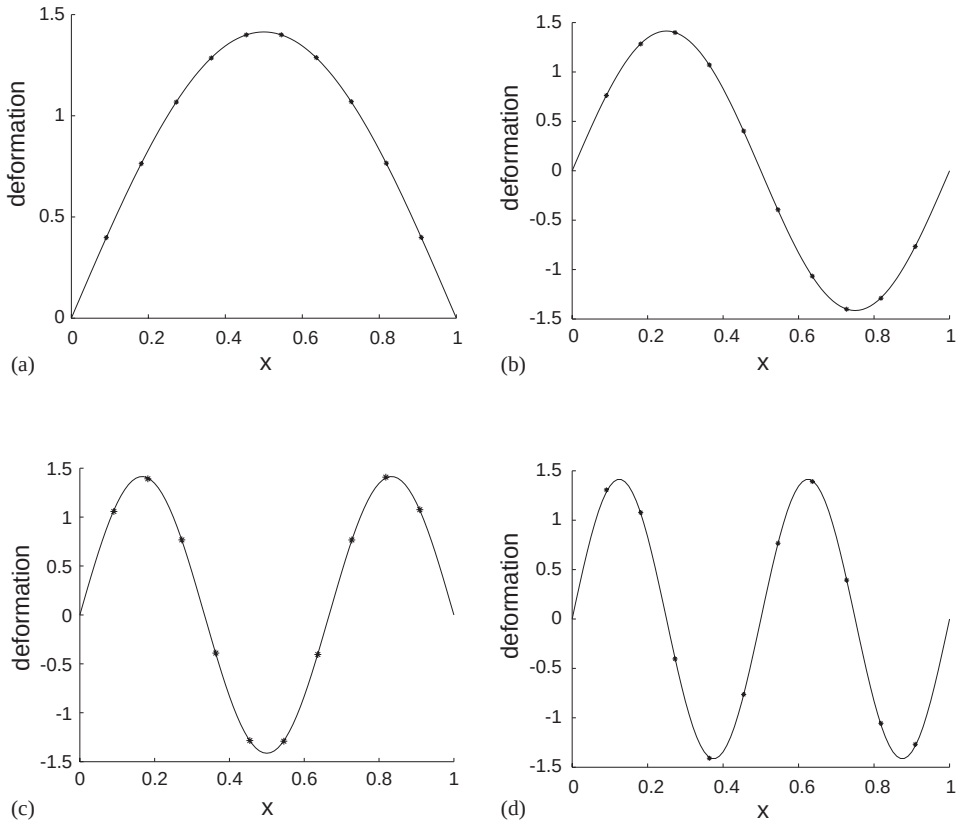

Fig. 2. The first four LNMs of an undamped hinged–hinged beam are plotted with solid lines, '—'. The corresponding POMs are plotted with symbols, '∗'. (a) First mode, (b) second mode, (c) third mode, and (d) fourth mode.

Fig. 3. The benefit of using redundant sensors for effectively better interpolation in the underlying orthogonality integral has been seen in experiments [20].

3.3. Damping and finite data

For our last examples, we look at the effect of damping. Intuitively, we might expect ongoing random excitation to continually renew the instantaneous modal participation, such that modal damping may not be an issue. However, Eq. (14), in its current form, does not guarantee the diagonalization of $\mathbf{R_Q}$ in the presence of damping, as $N \to \infty$. In practice, N is finite. Eq. (14), and past experience with impulse responses [3], suggest the interpretation to hold if the damping is light. However, if the damping is "large", particularly if $\zeta_i \geqslant 1$ and $h_i(t)$ are non-sinusoidal functions, we may not expect $\mathbf{R_Q}$ to approach diagonalization. In comparison, classical experimental modal analysis also calls for light damping, such that resonances are clearly defined.

Fig. 4 shows the first four identified mode shapes of the hinged beam for the case of modal damping ratios of 0.05 added to each mode in the simulation. As expected, light damping does not adversely effect the POD.

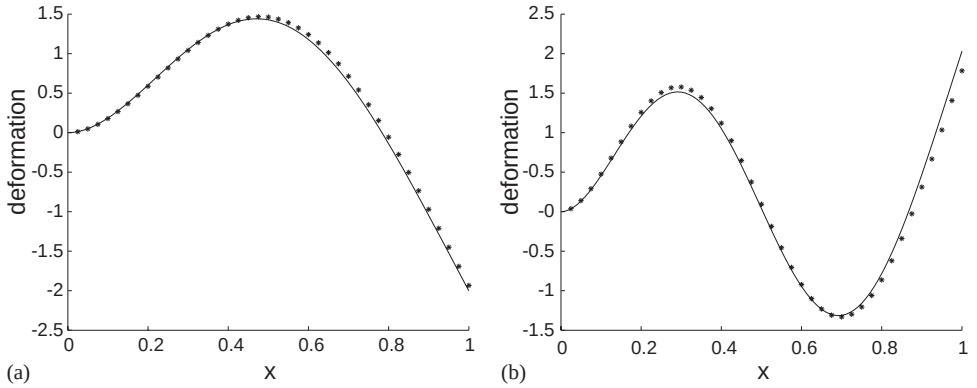

Fig. 3. The second and third modes of an undamped cantilevered beam are plotted with solid lines, '—'. The corresponding POMs drawn from 40 equally spaced sensors are plotted with asterisks, '∗'. (a) Second mode and (b) third mode.

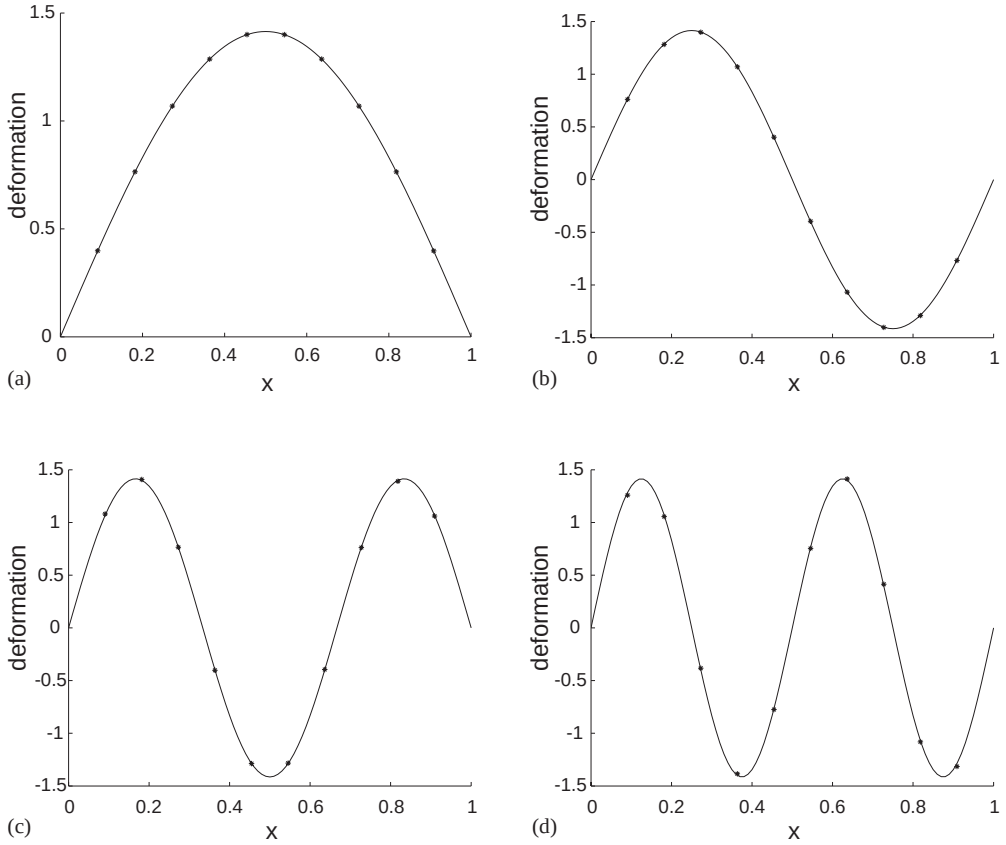

Fig. 4. The first four LNMs of a hinged–hinged beam are plotted with solid lines, '—'. The corresponding POMs computed from response data with modal damping of $\zeta = 0.05$ for each mode are plotted with symbols, '∗'. (a) First mode, (b) second mode, (c) third mode, and (d) fourth mode.

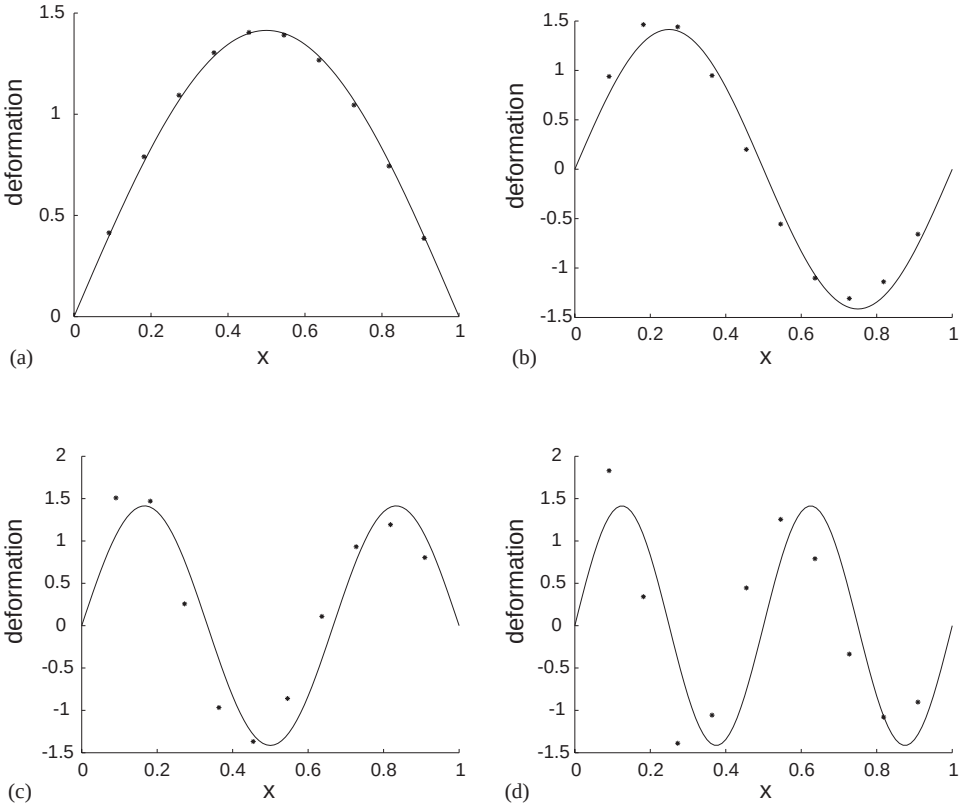

Fig. 5. The first four LNMs of a hinged–hinged beam are plotted with solid lines, '—'. The corresponding POMs computed from response data with modal damping of $\zeta = 1$ for each mode are plotted with symbols, '$*$'. (a) First mode, (b) second mode, (c) third mode, and (d) fourth mode.

Fig. 5 shows the first four identified modes of the hinged beam for the case of critical damping imposed on each mode during the simulation. The deviation of the POMs from the LNMs is small for the first mode, but becomes substantial as the modes increase, indicating the importance of a sinusoidal characteristic in the modal impulse-response functions $h_i(t)$, and their role in Eq. (14).

4. Conclusion

We have a relationship between the proper orthogonal modes and modes of vibration of homogeneous lumped parameter and continuous parameter systems under random excitation. This extends previous results for multi-modal free responses (or impulse responses).

Under random excitation with a convergent Fourier transform, which means zero mean and no sustained sinusoidal components, the POMs converge to the LNMs in lumped parameter models, and the POMs approximate the discretized LNMs of distributed systems if the discretization is evenly spaced. The quality of the approximation is partly dependent on how well the integral

orthogonality property of the modal functions transfers to the discretized modal vectors, for which the inner product can be seen as proportional to a rectangular-rule integration.

The mass distribution must be known to make these conclusions, and the problem must be formulated in displacement co-ordinates defined such that the associated mass distribution is uniform.

The results were tested on a three-mass system, a cantilevered beam and a hinged–hinged beam. The role of damping was briefly touched through examples. The theory supports the usage of POD for estimating LNMs when the modal damping is "light". When the damping is large, the POMs deviate from the LNMs.

In short, we have worked toward establishing a bridge between statistically derived POMs and the geometry of normal modes, in the case of random excitation. This complements a recent tie made for impulse responses. The broad goal is to open the door for POD to be applied as a modal analysis tool. To make this goal a reality, developments are needed to overcome the requirement for a known mass distribution.

Acknowledgements

This work was supported by a grant from the National Science Foundation (CMS-0099603). We appreciate discussions with Prof. Alan Haddow on issues surrounding Fourier transforms of time-series data.

References

[1] G. Berkooz, P. Holmes, J.L. Lumley, The proper orthogonal decomposition in the analysis of turbulent flows, Annual Review of Fluid Mechanics 25 (1993) 539–575.

[2] J.P. Cusumano, M.T. Sharkady, B.W. Kimble, Spatial coherence measurements of a chaotic flexible-beam impact oscillator, in: J.P. Casumano, C. Pierre, S.T. Wu (Eds.), Aerospace Structures: Nonlinear Dynamics and System Response, ASME (American Society of Mechanical Engineers), New York, AD-Vol. 33, 1993, pp. 13–22.

[3] B.F. Feeny, R. Kappagantu, On the physical interpretation of proper orthogonal modes in vibrations, Journal of Sound and Vibration 211 (4) (1998) 607–616.

[4] J.L. Lumley, The structure of inhomogeneous turbulent flow, in: A.M. Yaglom, V.I. Tatarski (Eds.), Atmospheric Turbulence and Radio Wave Propagation, Nauka, Moscow, pp. 166–178.

[5] J.L. Lumley, Stochastic Tools in Turbulence, Academic Press, New York, 1970.

[6] J.P. Cusumano, B.-Y. Bai, Period-infinity periodic motions, chaos, and spatial coherence in a 10 degree of freedom impact oscillator, Chaos, Solitons, and Fractals 3 (5) (1993) 515–535.

[7] M.A. Davies, F.C. Moon, Solitons, chaos, and modal interactions in periodic structures, in: A. Guran (Ed.), Nonlinear Dynamics: The Richard Rand 50th Anniversary Volume, World Scientific, Singapore, 1997, pp. 119–143.

[8] I.T. Georgiou, I.B. Schwartz, E. Emaci, A.F. Vakakis, Interaction between slow and fast oscillations in an infinite degree-of-freedom linear system coupled to a nonlinear system: theory and experiment, Journal of Applied Mechanics 66 (2) (1999) 448–459.

[9] P. FitzSimons, C. Rui, Determining low dimensional models of distributed systems, in: E.A. Misawa (Ed.), Advances in Robust and Nonlinear Control Systems, ASME, New York, DSC-Vol. 53, 1993, pp. 9–15.

[10] R. Kappagantu, B.F. Feeny, An 'optimal' modal reduction of a system with frictional excitation, Journal of Sound and Vibration 224 (5) (1999) 863–877.

[11] R.V. Kappagantu, B.F. Feeny, Part 2: proper orthogonal modal modeling of a frictionally excited beam, Nonlinear Dynamics 23 (1) (2000) 1–11.
[12] X. Ma, A.F. Vakakis, Nonlinear transient localization and low dimensional models of a flexible system with a clearance, in: ASME Design Engineering Technical Conferences, Las Vegas, NV, CD-ROM, 1999.
[13] X. Ma, M.A.F. Azeez, A.F. Vakakis, Nonlinear normal modes and nonparametric system identification of nonlinear oscillators, Mechanical Systems and Signal Processing 14 (1) (2000) 37–48.
[14] M.A.F. Azeez, A.F. Vakakis, Proper orthogonal decomposition (POD) of a class of vibroimpact oscillations, Journal of Sound and Vibration 240 (5) (2001) 859–890.
[15] K. Yasuda, K. Kamiya, Experimental identification technique of nonlinear beams in time domain, in: ASME Design Engineering Technical Conferences, Sacramento, on CD-ROM, 1997.
[16] V. Lenaerts, G. Kerschen, J.C. Golinval, Parameter identification of nonlinear mechanical systems using proper orthogonal decomposition, in: Proceedings of the IMAC XVIII, San Antonio, TX, 2000.
[17] O. Kust, Modal analysis of long torsional strings through proper orthogonal decomposition, Zeitschrift fuer angewandte Mathematik und Mechanik 77 (S1) (1997) S183–S184.
[18] G. Kerschen, J.C. Golinval, Physical interpretation of the proper orthogonal modes using singular value decomposition, Journal of Sound and Vibration 249 (5) (2002) 849–866.
[19] B.F. Feeny, On the proper orthogonal modes and normal modes of continuous vibration systems, Journal of Vibration and Acoustics 124 (1) (2002) 157–160.
[20] M.S. Riaz, B.F. Feeny, Proper orthogonal modes of a beam sensed with strain gages, Journal of Vibration and Acoustics 125 (1) (2003) 129–131.
[21] S. Han, B. Feeny, Enhanced proper orthogonal decomposition for the modal analysis of homogeneous structures, Journal of Vibration and Control 8 (1) (2002) 19–40.
[22] D. Inman, Engineering Vibration, Prentice-Hall, Englewood Cliffs, NJ, 1994.
[23] G.E. Forsythe, M.A. Malcolm, C.B. Moler, Computer Methods for Mathematical Computations, Prentice-Hall, Englewood Cliffs, NY, 1977.
[24] S.S. Rao, Mechanical Vibrations, 3rd Edition, Addison-Wesley Publishing Company, Reading, MA, 1995, p. 849.
[25] M.A. Norris, S.P. Kahn, L.M. Silverberg, C.E. Hedgecock, The time correlation method for modal identification of lightly damped structures, Journal of Sound and Vibration 162 (1) (1993) 137–146.